PHYSICAL REVIEW B **91**, 161403(R) (2015)

Tunable terahertz frequency comb generation using time-dependent graphene sheets

Vincent Ginis,[1] Philippe Tassin,[2,*] Thomas Koschny,[3] and Costas M. Soukoulis[3,4]
[1]*Applied Physics Research Group (APHY), Vrije Universiteit Brussel, Pleinlaan 2, B-1050 Brussel, Belgium*
[2]*Department of Applied Physics, Chalmers University, SE-412 96 Göteborg, Sweden*
[3]*Ames Laboratory—U.S. DOE and Department of Physics and Astronomy, Iowa State University, Ames, Iowa 50011, USA*
[4]*Institute of Electronic Structure and Lasers (IESL), FORTH, GR-71110 Heraklion, Crete, Greece*
(Received 1 March 2014; revised manuscript received 10 March 2015; published 8 April 2015)

We investigate the interaction between electromagnetic pulses and two-dimensional current sheets whose conductivity is controlled as a function of time by the generation of photocarriers, and we discuss its applicability to tunable frequency comb generation. To this aim, we develop an analytical model that permits the calculation of the scattered waves off a thin sheet with time-dependent, dispersive sheet conductivity. We evaluate the transmitted spectrum as a function of the dispersive behavior and the modulation frequency of the number of photocarriers. We conclude that such active materials, e.g., time-dependent graphene sheets, open up the possibility to manipulate the frequency of incident pulses and, hence, could lead to highly tunable, miniaturized frequency comb generation.

DOI: 10.1103/PhysRevB.91.161403 PACS number(s): 78.20.Ci, 78.67.Pt, 72.80.Vp, 42.70.Qs

Ever since the invention of the laser, scientists have tried to increase the upper limit of frequency measurements from radio frequencies to the optical domain [1]. The development of optical frequency combs [2,3]—sharp, evenly spaced spectral lines with a fixed phase relation between adjacent comb lines [4,5]—simplified these measurements considerably and paved the way for accurate frequency measurements in the optical domain [6,7]. As of today, frequency combs offer the precision required for the conception of optical clocks [8], and they are used in a plethora of disciplines, including atomic [9] and molecular spectroscopy [10], calibration of spectrometers in astronomical observations [11], infrared chemical sensing [12], ultraviolet spectroscopy [13], attosecond pulse generation [14], and even the determination of the temporal stability of fundamental physical constants [15].

Optical frequency combs are normally generated with mode-locked lasers, in which a fixed phase relation is imposed on the longitudinal modes of a laser with a large gain bandwidth, e.g., Ti:sapphire lasers [16] or fiber lasers [17]. This can be achieved by inserting an electro-optical modulator or a saturable absorber inside the laser cavity. The temporal separation between consecutive pulses then equals the round-trip time of the laser cavity t_{rep}. In order to obtain even broader output spectra, these lasers are often combined with nonlinear microstructured photonic crystal fibers of which the group velocity dispersion properties can be engineered [18,19]. Recently, a novel approach for frequency comb generation, based on parametric frequency conversion inside compact high-Q microresonators, has emerged [20]. In comparison with the traditional comb sources, this technique allows for the reduction of the source footprint, an enhancement of the repetition frequency [21], and a larger tunability of the pump laser frequency [22].

In this Rapid Communication, we introduce another approach for frequency comb generation based on the interaction of an electromagnetic pulse with a thin-film interface whose conductivity is rapidly modulated as a function of time. Indeed, in recent years, scientists have extended the physics and applications of structured electromagnetic systems [23–29] towards tunable structures [30–35], e.g., by inclusion of electrically biased semiconductors, semiconductors with induced photocarriers, or graphene sheets in the design of metamaterials. Here, we show how rapidly tunable surfaces allow for the generation of highly miniaturized, tunable frequency comb generation. To this aim, we first derive a general formalism for the calculation of transmitted and reflected fields off time-dependent sheets with Drude dispersion.

We calculate the reflected (subscript R) and transmitted (subscript T) fields excited by an arbitrary incident pulse (subscript I) on a time-varying thin-film material. The electric field $\mathbf{E}$ and the magnetic field $\mathbf{H}$ are related to the electromagnetic vector potential $\mathbf{A}$. We choose the Coulomb gauge, so that the electrostatic potential in vacuum equals zero and, therefore, that $\mathbf{E} = -\partial\mathbf{A}/\partial t$. We consider oblique incident transverse electric waves on a surface perpendicular to the x axis and we explicitly invoke the vacuum dispersion relation by assuming the argument of the fields to be equal to $(t - k_x x/\omega - k_y y/\omega)$ for the incident and transmitted fields and $(t + k_x x/\omega - k_y y/\omega)$ for the reflected fields. Since the sheet is isotropic and nonchiral, the polarization of the fields does not change and we can write that $\mathbf{A}_{\{I,R,T\}} = G_{\{I,R,T\}}\mathbf{1_z}$. Defining $\partial G(\alpha)/\partial\alpha = \dot{G}(\alpha)$, we can express the tangential electric and magnetic fields as $\mathbf{E}^{\parallel}_{\{I,R,T\}}(x,t) = -\dot{G}(\alpha)\mathbf{1_z}$, $\mathbf{H}^{\parallel}_{\{I,T\}}(x,t) = -\eta^{-1}\dot{G}(\alpha)\mathbf{1_y}$, and $\mathbf{H}^{\parallel}_{\{R\}}(x,t) = \eta^{-1}\dot{G}(\alpha)\mathbf{1_y}$, where the wave impedance η equals $\mu_0\omega/k_\perp$. To find the reflected and transmitted fields for an arbitrary incident wave, the electromagnetic boundary equations need to be evaluated at the interface of the thin sheet. In general, these equations are given by

$$E_{\mathrm{left}}(t) - E_{\mathrm{right}}(t) = j_{\mathrm{sm}}(t),$$
$$H_{\mathrm{left}}(t) - H_{\mathrm{right}}(t) = j_{\mathrm{se}}(t),$$

where we defined the electric and magnetic sheet currents as $\mathbf{j}_{\mathrm{se}} = j_{\mathrm{se}}\mathbf{1_z}$ and $\mathbf{j}_{\mathrm{sm}} = j_{\mathrm{sm}}\mathbf{1_y}$, respectively. Maxwell's boundary conditions in the time domain then become

$$-\dot{G}_I(t) - \dot{G}_R(t) + \dot{G}_T(t) = j_{\mathrm{sm}}(t), \quad (1)$$

$$-\dot{G}_I(t) + \dot{G}_R(t) + \dot{G}_T(t) = \eta j_{\mathrm{se}}(t). \quad (2)$$

*Corresponding author.

The solutions, i.e., the reflected and transmitted fields, can only be found after inserting constitutive relations describing the coupling between the electric and magnetic currents on one hand and the electric and magnetic fields on the other hand. Below, we will solve this problem for sheets with dispersionless, time-dependent conductivities, as well as for sheets with a time-dependent electric conductivity with Drude dispersion.

When the scattering time scale of the carriers is sufficiently smaller than the modulation time scale, we can resort to the approximation that the sheet has dispersionless conductivities $j_{se}(t) = \sigma_{se}(t)E_{loc}(t)$ and $j_{sm}(t) = \sigma_{sm}(t)H_{loc}(t)$, where σ_{se} and σ_{sm} are the electric and magnetic sheet conductivities, respectively. The electric and magnetic sheet currents introduce a discontinuity in the magnetic and electric fields. Therefore, the constitutive equations relate the surface currents to the local fields on the surface (E_{loc} and H_{loc}), which equal the average of the tangential fields across the surface [36]. Inserting these constitutive relations into Eqs. (1) and (2) yields the transmitted and reflected fields given by

$$\dot{G}_T(t) = \frac{4 - \sigma_{se}(t)\sigma_{sm}(t)}{[2 + \eta\sigma_{se}(t)][2 + \sigma_{sm}(t)/\eta]}\dot{G}_I(t), \tag{3}$$

$$\dot{G}_R(t) = \frac{2[\sigma_{se}(t)\eta - \sigma_{sm}(t)/\eta]}{[2 + \eta\sigma_{se}(t)][2 + \sigma_{sm}(t)/\eta]}\dot{G}_I(t). \tag{4}$$

Subsequently, we consider a constitutive relation that includes dispersion and explicit time dependence in the electric currents, but with vanishing magnetic currents. This constitutive relation accurately describes the behavior of a graphene layer in which the number of photocarriers is modulated as a function of time,

$$j_{se}(t) = \int_{-\infty}^{+\infty} \sigma_{se}(t-u,t)E(u)du,$$

$$\sigma_{se}(t-u,t) = \frac{\sigma_0(t)}{\tau}\exp\left(-\frac{t-u}{\tau}\right)h(t-u),$$

where $h(t)$ is the Heaviside step function. When we insert this constitutive relation in Maxwell's boundary conditions, we obtain a Volterra integral equation of the second kind [37] for the transmitted field. Its solutions are given by

$$\dot{G}_T(t) = \dot{G}_I(t) - \frac{\eta}{2}\int_{-\infty}^{t}\frac{\sigma_0(t)}{\tau}\exp\left(-\frac{t-u}{\tau}\right) \times \exp\left(-\frac{\eta}{2\tau}\int_u^t \sigma_0(s)ds\right)\dot{G}_I(u)du. \tag{5}$$

We show in the Supplemental Material [38] that Eq. (5) is compatible with the traditional transmission formulas that arise in the limits of time-dependent nondispersive carriers and time-invariant dispersive carriers. We note that, in the nondispersive as well as in the dispersive case, the surface conductivity is multiplied with the sheet impedance η. Therefore, it is possible to trade in the amplitude of the conductivity variation for a larger angle of the oblique incident waves.

We now apply the previously derived formulas to evaluate the field that is transmitted through an interface with time-dependent conductivity, and we demonstrate how sheets with time-dependent electrical conductivity allow for frequency sideband generation at integral multiples of the modulation

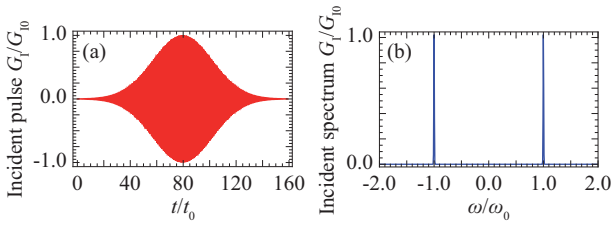

FIG. 1. (Color online) The incident pulse that is used to calculate the transmitted spectra of different time-dependent surfaces. (a) In the time domain. The pulse is temporally broad ($\Delta t = 200/\omega_0$). (b) In the frequency domain. The Gaussian pulse is nearly monochromatic.

frequency. In all subsequent simulations, we illuminate the sheet with a Gaussian pulse $G_I = \sin[\omega_0(t - t_{in})]\exp[-(t - t_{in})^2/\Delta t^2]$, where t_{in} is an arbitrary time shift, ω_0 is the center frequency, and the pulse width Δt equals $200/\omega_0$. This pulse is visualized both in the time domain and in the frequency domain in Fig. 1. In these and subsequent plots we nondimensionalized the abscissa using $t_0 = 2\pi/\omega_0$ and ω_0. We start with the nondispersive interface, evaluating Eq. (3). We modulate the electric conductivity of the conductive sheet with the sinusoidal profile

$$\sigma_0(t) = \frac{\sigma_{max} - \sigma_{min}}{2}\sin(\omega_{mod}t + 0.2) + \frac{\sigma_{max} + \sigma_{min}}{2}, \tag{6}$$

which oscillates between the minimal conductivity $\sigma_{min} = 10^{-8}$ S and the maximal conductivity $\sigma_{max} = 100$ mS with frequency $\omega_{mod} = \omega_0/10$. The transmitted wave will then be a sampled version of the incident pulse, generating a pulse train at fixed separation intervals, in agreement with the modulation period $t_{mod} = 2\pi/\omega_{mod}$, as shown in Fig. 2(a). In the frequency domain this transmitted signal corresponds to a comb of frequencies, where the incident spectrum—originally centered around ω_0—is copied at several sideband frequencies located at $\omega_n = \omega_0 + n\omega_{mod}$ [see Fig. 2(b)]. The amplitude of the spectrum decreases at higher frequencies as a result of the finite sampling inherent to a sinusoidal modulation.

To investigate the effects of non-negligible dispersion of the photocarriers, we evaluate Eq. (5) to calculate the field transmitted through an interface whose conductivity modulation is given by Eq. (6). This is, e.g., necessary when the Drude scattering time τ of the photocarriers is larger than the optical cycle of the incident pulse. In Fig. 3, we

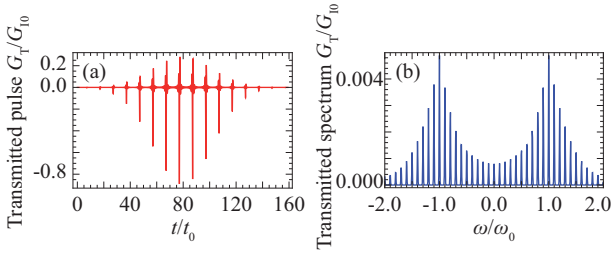

FIG. 2. (Color online) The transmitted wave through a nondispersive sheet whose time-dependent electrical conductivity is modulated according to Eq. (6). (a) In the time domain, we observe a train of very sharp pulses that are separated by the modulation period t_{mod}. (b) In the frequency domain, this corresponds to a frequency comb.

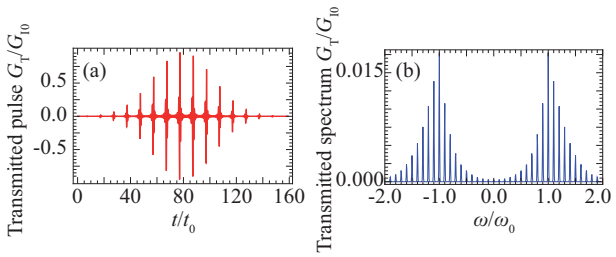

FIG. 3. (Color online) The transmitted wave (a) in the time domain and (b) in the frequency domain through a time-dependent sheet with photocarrier modulation given by Eq. (6) in which the dispersion of the photocarriers is significant ($\tau = \pi/\omega_0$).

plot the transmitted field through a dispersive sheet with a collision frequency $\gamma = \omega_0/\pi$. The output still corresponds to a frequency comb, with the incident spectrum copied at integral multiples of the modulation frequency ω_{mod} around the incident center frequency ω_0. However, in comparison with the transmitted wave in the nondispersive case (Fig. 2), the envelope decreases more rapidly. In return, the amplitude of the incident center frequency ω_0 is larger in the dispersive case than in the nondispersive case. This indicates that less energy is spread from the central peak to the sidebands.

This trend is confirmed when we compare even higher scattering times τ, as demonstrated in Fig. 4 in which we plot the temporal and spectral representation of the transmitted pulse through two distinct sheets with different relaxation times, $\tau = 2\pi/\omega_0$ in Figs. 4(a) and 4(b) and $\tau = 8\pi/\omega_0$ in Figs. 4(c) and 4(d). By comparing Fig. 4(b) with Fig. 4(d), it is clear that the spectral envelope narrows down as the material response time increases. In the time domain, this behavior translates into transmitted pulses that are less sharp as τ increases.

Finally, we discuss the influence of the modulation frequency ω_{mod} on the spectrum of the transmitted pulse. In agreement with the intuitive sampling model of the time-dependent sheet, this modulation frequency directly corresponds to the spacing of the sidebands in the transmitted spectrum, even

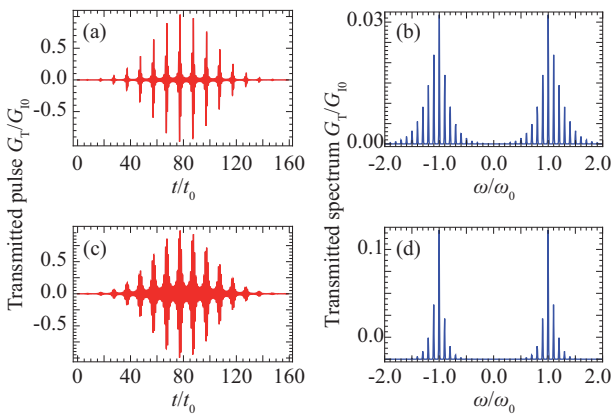

FIG. 4. (Color online) Transmitted waves in the time domain and in the frequency domain for different relaxation times of the photocarriers: $\tau = 2\pi/\omega_0$ in (a) and (b), and $\tau = 8\pi/\omega_0$ in (c) and (d). $\omega_{\text{mod}} = 0.1\omega_0$ in both simulations.

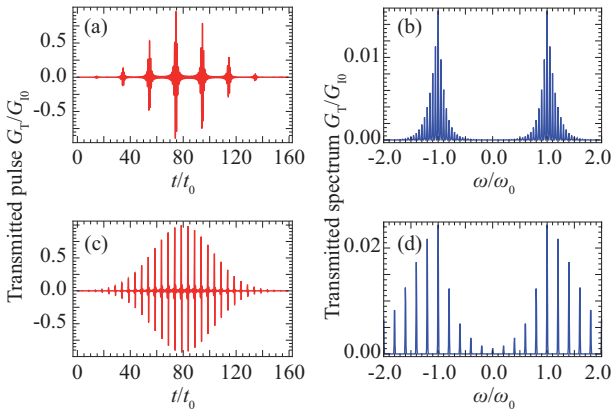

FIG. 5. (Color online) Transmitted waves in the time domain and in the frequency domain for different modulation frequencies of the photocarriers: $\omega_{\text{mod}} = 0.05\omega_0$ in (a) and (b), and $\omega_{\text{mod}} = 0.2\omega_0$ in (c) and (d). $\tau = \pi/\omega_0$ in both simulations.

when considering a significant relaxation time $\tau = \pi/\omega_0$. This is shown in Fig. 5, where we compare the transmitted pulses of two sheets in which the photocarrier concentrations are modulated at a frequency $\omega_{\text{mod}} = 0.05\omega_0$ and $\omega_{\text{mod}} = 0.2\omega_0$, respectively.

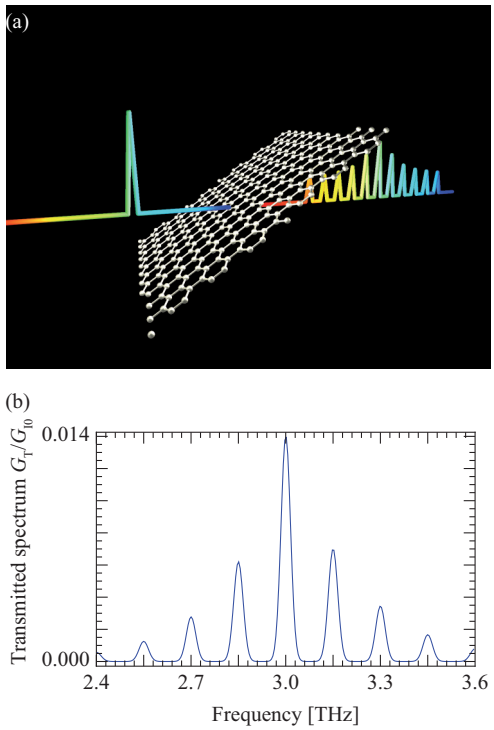

FIG. 6. (Color online) (a) An illustration of the proposed mechanism for highly tunable frequency comb generation using graphene sheets. The sheet conductivity of the graphene sample is modeled using a Drude response, retrieved from experimental data [41]: $\sigma_{\text{max}} = 28$ mS and $\tau = 167$ fs. (b) The resulting transmitted spectrum through the graphene sheet. Even when the considerable dispersion of the graphene photocarriers is taken into account, a quasimonochromatic pulse can be converted into a frequency comb.

The previous results are in agreement with our qualitative picture that a sheet with modulated photocarriers acts as a time-dependent shutter. In the rather academical example of dispersionless carriers, the spectrum of the transmitted field constitutes a frequency comb, in which the incident spectrum is copied at several sideband frequencies at a fixed separation frequency ω_{mod}. When realistic dispersion is added to the carrier dynamics of the conducting system, the desired properties of the transmitted spectrum remain present. Qualitatively, the introduction of dispersion merely narrows the spectral envelope that limits the overall bandwidth of the frequency comb. In addition, we have shown that the sideband spacing can be tuned by changing the modulation frequency of the photocarriers.

Although the main point of this Rapid Communication is to theoretically propose a new idea for tunable frequency comb generation, we conclude with a brief discussion of the experimental feasibility of the proposed mechanism. Given the ability to modulate its carrier density at very high frequencies [39], graphene offers an attractive platform for tunable frequency comb generation. Moreover, at terahertz frequencies, the electronic response of graphene is essentially that of a free-electron Drude gas [40]. In Fig. 6, we present a typical frequency comb that can be transmitted through a graphene sheet. To obtain this figure, we inserted experimental data for the sheet conductivity of graphene, i.e., $\sigma_{\mathrm{max}} = 28$ mS and $\tau = 167$ fs in our model [41]. The resulting frequency comb is centered around 3 THz and has a comb line spacing of 150 GHz. Figure 6 demonstrates that, even with contemporary available graphene samples, the proposed mechanism can be exploited to generate tunable frequency combs at terahertz frequencies. To further increase the bandwith of the resulting combs, we expect that geometrically patterned graphene sheets [42] or other structured metasurfaces with a resonant response will be used to enhance the maximum surface conductivity. Another alternative would be the use of GaAs substrates with photoinduced carriers, whose modulation bandwidth is limited by the carrier recombination to a few gigahertz [43]. This makes them an attractive candidate for frequency comb generation at microwave frequencies.

The main advantage of our approach for the generation of frequency combs is its enhanced tunability. Indeed, the comb repetition frequency as well as the comb linewidth can be controlled by the modulation beam and the incident laser pulse, respectively. In this way, the same sheet could serve for the generation of frequency combs with different mode spacings, spectral linewidths, and overall bandwidths.

Work at the VUB (simulations) was supported by BelSPO (Grant No. IAP P7-35 photonics@be) and the Research Foundation—Flanders (Grant No. K2.185.13N). Work at Ames Lab (theory) was supported by the US Department of Energy, Office of Basic Energy Science, Division of Materials Sciences and Engineering under Contract No. DE-AC02-07CH11358). Work at FORTH (modeling) was supported by the European Research Council under ERC Advanced Grant No. 320081 (PHOTOMETA). V.G. acknowledges support as a Fellow of the Research Foundation—Flanders (FWO-Vlaanderen).

[1] A. Szöke and A. Javan, Phys. Rev. Lett. **10**, 521 (1963).
[2] J. L. Hall, Rev. Mod. Phys. **78**, 1279 (2006).
[3] T. W. Hänsch, Rev. Mod. Phys. **78**, 1297 (2006).
[4] T. Udem, R. Holzwarth, and T. W. Hänsch, Nature (London) **416**, 233 (2002).
[5] S. T. Cundiff and J. Ye, Rev. Mod. Phys. **75**, 325 (2003).
[6] R. Holzwarth, T. Udem, T. W. Hänsch, J. C. Knight, W. J. Wadsworth, and P. S. J. Russell, Phys. Rev. Lett. **85**, 2264 (2000).
[7] S. A. Diddams, D. J. Jones, J. Ye, S. T. Cundiff, J. L. Hall, J. K. Ranka, R. S. Windeler, R. Holzwarth, T. Udem, and T. W. Hänsch, Phys. Rev. Lett. **84**, 5102 (2000).
[8] M. Takamoto, F.-L. Hong, R. Higashi, and H. Katori, Nature (London) **435**, 321 (2005).
[9] T. Hänsch, J. Alnis, P. Fendel, M. Fischer, C. Gohle, M. Herrmann, R. Holzwarth, N. Kolachevsky, T. Udem, and M. Zimmermann, Philos. Trans. R. Soc., A **363**, 2155 (2005).
[10] S. A. Diddams, L. Hollberg, and V. Mbele, Nature (London) **445**, 627 (2007).
[11] T. Steinmetz, T. Wilken, C. Araujo-Hauck, R. Holzwarth, T. W. Hnsch, L. Pasquini, A. Manescau, S. D'Odorico, M. T. Murphy, T. Kentischer, W. Schmidt, and T. Udem, Science **321**, 1335 (2008).
[12] A. Schliesser, M. Brehm, F. Keilmann, and D. van der Weide, Opt. Express **13**, 9029 (2005).
[13] C. Gohle, T. Udem, M. Herrmann, J. Rauschenberger, R. Holzwarth, H. A. Schuessler, F. Krausz, and T. W. Hänsch, Nature (London) **436**, 234 (2005).
[14] A. Baltuška, T. Udem, M. Uiberacker, M. Hentschel, E. Goulielmakis, C. Gohle, R. Holzwarth, V. S. Yakovlev, A. Scrinzi, T. W. Hänsch, and F. Krausz, Nature (London) **421**, 611 (2003).
[15] M. Hori, A. Dax, J. Eades, K. Gomikawa, R. S. Hayano, N. Ono, W. Pirkl, E. Widmann, H. A. Torii, B. Juhász, D. Barna, and D. Horváth, Phys. Rev. Lett. **96**, 243401 (2006).
[16] L. Matos, D. Kleppner, O. Kuzucu, T. R. Schibli, J. Kim, E. P. Ippen, and F. X. Kaertner, Opt. Lett. **29**, 1683 (2004).
[17] B. R. Washburn, S. A. Diddams, N. R. Newbury, J. W. Nicholson, M. F. Yan, and C. G. Jørgensen, Opt. Lett. **29**, 250 (2004).
[18] J. K. Ranka, R. S. Windeler, and A. J. Stentz, Opt. Lett. **25**, 25 (2000).
[19] J. M. Dudley, G. Genty, and S. Coen, Rev. Mod. Phys. **78**, 1135 (2006).
[20] P. Del'Haye, A. Schliesser, O. Arcizet, T. Wilken, R. Holzwarth, and T. J. Kippenberg, Nature (London) **450**, 1214 (2007).
[21] T. J. Kippenberg, R. Holzwarth, and S. A. Diddams, Science **332**, 555 (2011).
[22] P. Del'Haye, T. Herr, E. Gavartin, M. L. Gorodetsky, R. Holzwarth, and T. J. Kippenberg, Phys. Rev. Lett. **107**, 063901 (2011).
[23] D. R. Smith, J. B. Pendry, and M. C. K. Wiltshire, Science **305**, 788 (2004).
[24] R. Engheta and R. W. Ziolkowski, *Metamaterials, Physics and Engineering Explorations* (Wiley-IEEE, New York, 2006).
[25] C. M. Soukoulis and M. Wegener, Nat. Photonics **5**, 523 (2011).

[26] Y. Liu and X. Zhang, Chem. Soc. Rev. **40**, 2494 (2011).
[27] N. I. Zheludev and Y. S. Kivshar, Nat. Mater. **11**, 917 (2012).
[28] N. Yu, P. Genevet, M. A. Kats, F. Aieta, J.-P. Tetienne, F. Capasso, and Z. Gaburro, Science **334**, 333 (2011).
[29] C. L. Holloway, E. F. Kuester, J. A. Gordon, J. O'Hara, J. Booth, and D. R. Smith, IEEE Antennas Propag. Mag. **54**, 10 (2012).
[30] P. M. Johnson, A. F. Koenderink, and W. L. Vos, Phys. Rev. B **66**, 081102(R) (2002).
[31] W. J. Padilla, A. J. Taylor, C. Highstrete, M. Lee, and R. D. Averitt, Phys. Rev. Lett. **96**, 107401 (2006).
[32] H.-T. Chen, W. J. Padilla, J. M. Zide, A. C. Gossard, A. J. Taylor, and R. D. Averitt, Nature (London) **444**, 597 (2006).
[33] H.-T. Chen, J. F. O'Hara, A. K. Azad, A. J. Taylor, R. D. Averitt, D. B. Shrekenhamer, and W. J. Padilla, Nat. Photonics **2**, 295 (2008).
[34] N.-H. Shen, M. Massaouti, M. Gokkavas, J.-M. Manceau, E. Ozbay, M. Kafesaki, T. Koschny, S. Tzortzakis, and C. M. Soukoulis, Phys. Rev. Lett. **106**, 037403 (2011).
[35] C. Kurter, P. Tassin, A. P. Zhuravel, L. Zhang, T. Koschny, A. V. Ustinov, C. M. Soukoulis, and S. M. Anlage, Appl. Phys. Lett. **100**, 121906 (2012).
[36] P. Tassin, T. Koschny, and C. M. Soukoulis, Physica B **407**, 4062 (2012).
[37] A. D. Polyanin and A. V. Manzhirov, *Handbook of Integral Equations* (Chapman and Hall/CRC, Boca Raton, FL, 2008).
[38] See Supplemental Material at http://link.aps.org/supplemental/10.1103/PhysRevB.91.161403 for the derivation of the dispersive, time-dependent transmission formula and its reduction to two well-known limits.
[39] W. Li, B. Chen, C. Meng, W. Fang, Y. Xiao, X. Li, Z. Hu, Y. Xu, L. Tong, H. Wang *et al.*, Nano Lett. **14**, 955 (2014).
[40] J. Horng, C. Chen, B. Geng, C. Girit, Y. Zhang, Z. Hao, H. Bechtel, M. Martin, A. Zettl, M. Crommie *et al.*, Phys. Rev. B **83**, 165113 (2011).
[41] D. K. Efetov and P. Kim, Phys. Rev. Lett. **105**, 256805 (2010).
[42] P. Tassin, T. Koschny, and C. M. Soukoulis, Science **341**, 620 (2013)
[43] I. Chatzakis, P. Tassin, L. Luo, N.-H. Shen, L. Zhang, J. Wang, T. Koschny, and C. M. Soukoulis, Appl. Phys. Lett. **103**, 043101 (2013).